

## DETC2023- 116954 DRAFT

### TOWARDS HIGH DYNAMIC OPERATIONS WITH PARALLEL-SERIAL HYBRID ROBOTS

**Keerthi Sagar\***

Robotics and Automation<sup>1</sup>  
Irish Manufacturing Research Limited  
Mullingar, Ireland  
PMAR Robotics Group<sup>2</sup>  
University of Genoa  
Genoa, Italy 16145  
keerthi.sagar@imr.ie<sup>1</sup>  
keerthi.sagar.rao@edu.unige.it<sup>2</sup>

**Vishal Ramadoss**

PMAR Robotics Group  
University of Genoa  
Genoa, Italy 16145  
vishal.ramadoss@edu.unige.it

**Matteo Zoppi**

PMAR Robotics Group  
University of Genoa  
Genoa, Italy 16145  
matteo.zoppi@unige.it

#### **ABSTRACT**

*Hybrid manipulators are a combination of parallel and serial linkage connection robots which can exhibit high articulation and achieve modularity in design. This paper presents the results on the kinematic modeling and motion generation of a parallel-serial hybrid robot architecture. Parallel mechanisms are increasingly being employed as a reconfigurable subsystem alongside serial kinematic chains for high speed machining and manufacturing operations. These kinematic structures have known to have superior stiffness and dynamic properties at the expense of increased complexity in modeling and control. For a specific application of placing fixture heads along sheet metal, a hybrid parallel-serial manipulator is developed. It consists of a spherical revolute (SR) 4-degree-of-freedom (DOF) serial arm mounted on a (3-DOF) parallel manipulator with two UPR (4-DOF) legs constrained to move in a common rotating plane, and an SPR (5-DOF) leg. The kinematic architecture utilizes parallel linkage as a positioning manipulator, whereas the serial arm provides the necessary dexterity and increased workspace required for the task. An approach to model such complex kinematic structures with the evaluation of workspace and motion*

*generation is discussed. The presented approach is finally validated both in simulation and with experiments performed on the real platform.*

#### **1 Introduction**

The development of parallel kinematic machines (PKM) with reduced degrees of freedom (DOF), frequently three or four DOF, capable of generating high velocities and accelerations have become a significant point of interest in the field of robotics. These highly dynamical PKMs are required for fast manipulation and assembly extending their applications to high speed machining and precise manufacturing operations. On the other hand, serial manipulators help to achieve larger operating workspace. Parallel-serial hybrid robots are defined as combination of parallel manipulators and series or tree type kinematic chains. The unification of these architectures to form a hybrid manipulator, helps to exploit the advantages from both the topologies.

Recently there has been an increasing interest in employing parallel mechanism architectures [1] [2] either as sub-modules with the serial architecture or as a primary manipulator combined with the serial manipulator. The former being part of the series parallel hybrid robots which are discussed in [2] and the latter be-

---

\*Address all correspondence to this author.

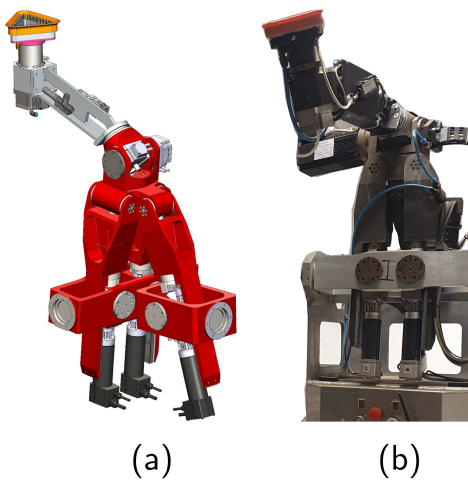


**FIGURE 1:** Hybrid parallel-serial architecture a) CAD Model b) Physical Prototype

ing parallel-serial hybrid robots that are studied in [3]. There is a need to resolve the kinematic complexity that is inherited from both topologies in a systematic way. In this article, we will investigate the kinematics and operational space motion generation of such parallel-serial hybrid robot. Fig. (1), shows the digital CAD model and a fabricated prototype of the robot architecture that is discussed in this article.

Many parallel-serial hybrid designs, primarily in the field of parallel robotics [4] [5], have been developed in the previous years. Romdhane [6] presents a mechanism with a base and two platforms namely mid platform and top platform assembled in series. The mid platform performs motion restricted to only three translations and the top platform with a spherical joint can provide additional relative motion between these two platforms, hence enabling 6-DOF with respect to the base. The advantages of such a mechanism is that, a closed-form solution is achieved enabling the capability to determine all possible solutions for the forward analysis and also having the size of the orientation workspace independent of the position of the top platform, which is not the case in fully parallel mechanisms. For a similar hybrid structure, Tanev [7] presents a kinematic analysis of two serially connected parallel mechanisms.

Zhou *et al.* [3] introduced a 3-DOF hybrid robotic manipulator which combines a parallel mechanism and a pantograph to increase stiffness capabilities. A combination of parallel manipulator with serial chain is proposed by Lee *et al.* [8] for a propeller grinding application. For a similar architecture, Huang *et al.* [9] provides detailed study on the velocity kinematics. These hybrid structures combine the advantages of parallel and serial manipulators to achieve improved stiffness and manipulability [10] and also provide great advantage from a rigidity and workspace per-

spective [8].

In this work, we explore in detail the combination of a widely known PKM architecture- Exechon and serial architecture to be applied as a fixturing device. In previous work, the inverse kinematics [11] and direct kinematics [11–13] have been analyzed for the Exechon manipulator and detailed inverse kinematic analysis has been developed by Zoppi *et al.* [14]. The contributions of this work can be summarized as follows:

- Complete kinematic solution for serial and parallel manipulator for hybrid manipulator is presented.
- Reachable workspace boundary to compute the necessary bounds for both the positional manipulator as well as the univocal parameter range to be used in trajectory planning is derived.
- A complete parametric model is presented with the main intent of providing an algorithmic methodology for overall design in the direction of integrated analysis tools.

## 2 DESCRIPTION OF THE HYBRID ARCHITECTURE

The conceptual design of the hybrid parallel-serial architecture is shown in Fig. (2). Here, the graph based kinematic topology is clearly represented. The parallel robot [15] consists of three legs with a moving platform. The parallel robot is used as a regional manipulator (a 3-DOF positioning device). The first leg consists of a 5-DOF spherical-prismatic-revolute (SPR) chain and the other two legs are identical with 4-DOF universal-prismatic-revolute (UPR) joints. The two identical legs are constrained to move in a common rotating plane. The prismatic joints are actuated in the three legs and the rest of the joints are passive. The serial chain consists of a spherical joint like architecture with three- rotary actuators that provides higher manipulation capability for the end-effector head and a redundant revolute joint without any passive joints. The redundant revolute joint along the end-effector provides additional orientational capabilities. The significance of the revolute joint is to position triangular fixture heads along a contour, while they satisfy the constraints of being adequately close to the machining contour and also avoid collision between multiple manipulators and between the tool and the end-effector head. The revolute joint provides accurate and fast positioning for this specific use-case scenario.

This architecture was developed for a specific application of fixturing large sheet metals. The manipulator was designed and prototyped to operate as a reconfigurable fixture in aerospace manufacturing. Fig. (1) shows the assembly and the prototype developed. This particular design was chosen to appropriately locate fixturing heads by providing adequate stiffness by opposing the forces of the cutting tool. The parallel robot is equipped with electronically commutated Maxon EC 45 brushless motor with nominal speed at 4300 RPM and continuous peak torque of 331 Nm. The proposed hybrid robot has 7 DOFs, thus 7 motors

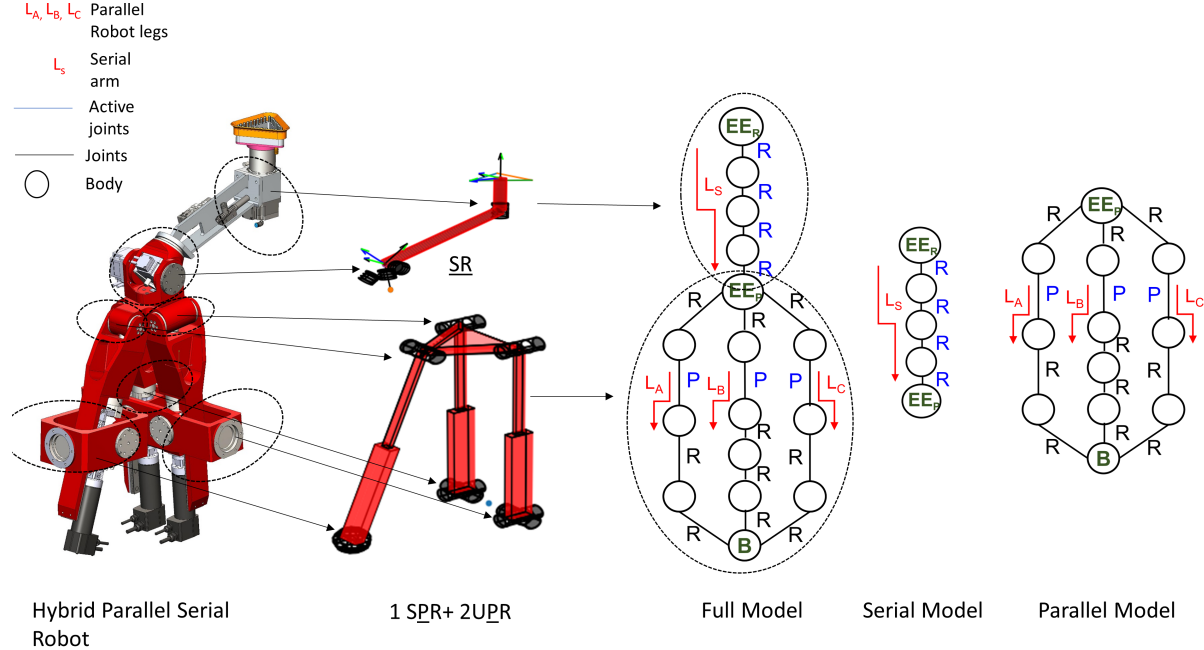


**FIGURE 2:** Hybrid Parallel Serial Architecture of 4-DOF SR arm mounted on a 3-DOF Exechon with its kinematic graphs.  $B$ ,  $EE_P$  and  $EE_R$  denotes the base, end-effector of the parallel manipulator and the end-effector of the serial spherical-revolute arm respectively. The underlined letters in the scheme denotes actuated joints.

and EPOS2 controllers are used. The serial chain is equipped with MOOG brushless servomotor, class F rated with 0.47 Nm rated torque at locked rotor and continuous peak torque as 2.6 Nm. The interpolated position mode in the CanOpen/CiA DSP v3.0 is utilized as the mode of operation in the EPOS2 controller. Considering the parallel manipulator model of the hybrid robot, the end-effector has three DOF. To understand the motion pattern of the moving platform, the concept of equivalent mechanism is adapted. The equivalent mechanism is a serial or a parallel kinematic chain whose moving platform has the given prescribed motion pattern. This allows us to parameterize the three joint freedoms in an univocal way locally. A simple linkage that reproduces the exact motion pattern of parallel manipulator is a quasi-serial chain with three joints, with its first joint visualized by a 1-DOF 2-RP planar parallel closed loop mechanism [14, 16], while the second and third joints are a revolute and prismatic pair, respectively. The equivalent linkage and its geometric relation to the current parallel chain is shown in Fig. (4a). The mathematical notations related to the kinematics of the hybrid architecture is shown in Fig. (3) and briefly discussed in the Nomenclature.

## 2.1 Inverse Kinematics: Parallel Chain

We briefly present the architecture of the Exechon and refer readers to [14] for a detailed description of the inverse kinematics (IK) for a generalized Exechon PKM. The two-identical legs

$L = A, C$  (RRPR) of the PKM share a common axis in their first base joint,  $\ell(\xi_1^A) = \ell(\xi_1^C)$ . The remaining two revolute joints are parallel to each other ( $\ell(\xi_2^L) \parallel \ell(\xi_4^L)$ ,  $L = \{A, C\}$ ). The active prismatic joints are perpendicular to the second and final revolute joint, i.e.,  $\ell(\xi_i^L) \perp \ell(\xi_3^L)$ ,  $i = (2, 4), L = A, C$ . The non-identical third leg (SPR), has a spherical joint at the base of the leg  $P_1^B$  and contains a passive revolute joint  $P_5^B$  at the tip of the leg with an axis perpendicular to the terminal joints of the other two-identical legs where,  $\ell(\xi_5^B) \perp \ell(\xi_4^L), L = (A, C)$ . Zoppi *et al.* [14], presented the motion pattern of Exechon-PKM using an equivalent mechanism with a non-singular representation,  $e = (\alpha, \beta, h)$ . The pose of the PKM is univocally represented using  $e$ . In this paper, we only present the final relevant equations and for detailed understanding of the kinematic model, we direct the reader to the referred article [14]. Point  $P$  (shown in Fig. 3) represents the platform end-effector point of the Exechon PKM, where  $P$  can be located in a rotating plane  $\pi_\alpha$ , where  $\alpha$  describes the rotation of the plane. Similarly, angle  $\beta$  represents the planar orientation of the platform in  $\pi_\alpha$ . An additional parameter  $h$ , denotes the measure of translation of the platform from the spherical joint projection  $P_1^B$  onto the rotating plane  $\pi_\alpha$ . This is a direct simplification from the equivalent mechanism and these three parameters  $\alpha$ ,  $\beta$ ,  $h$  define the platform pose  $P$  in the base frame  $\mathbf{O}_{lb} \mathbf{j}_b \mathbf{k}_b$ . The Exechon architecture consists of an offset spherical wrist with a center  $S = (S_x, S_y, S_z)$ . The spherical wrist is offset by a

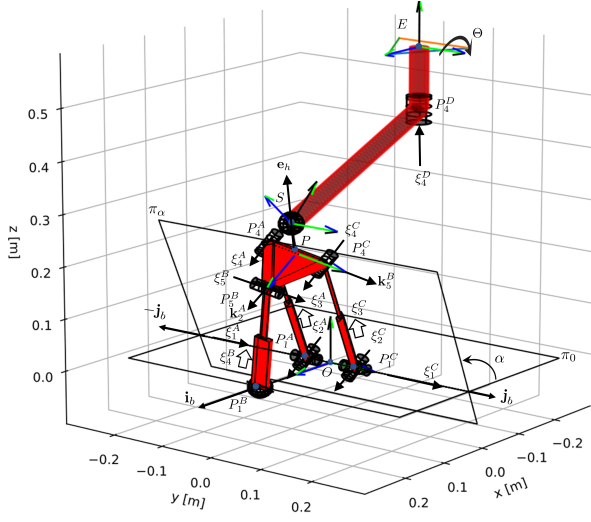


**FIGURE 3:** 4-DOF Spherical-Revolute (SR) arm mounted on a 3-DOF parallel manipulator. Green, blue, and black arrows represent  $\mathbf{i}, \mathbf{j}, \mathbf{k}$  basis vectors of their respective frames. Basis of the platform  $\mathbf{Pijk}$  are  $\mathbf{i} = \mathbf{k}_2^A = [s_\alpha, 0, s_\alpha]$ ,  $\mathbf{j} = \mathbf{k}_5^B = (P_1^B \mathbf{S} \times \mathbf{k}_2^A)$  &  $\mathbf{k} = \mathbf{n}_{12}^A = (\mathbf{i} \times \mathbf{j})$

distance  $h_z$  along the normal of the platform,  $\mathbf{n}_{12}^A = \mathbf{e}_h$ , and  $h_x$  along the  $\mathbf{i}$  basis vector of the exechon platform  $\mathbf{Pijk}$ . There exists four-working mode parameters for the Exechon PKM, where based on the choice of the spherical wrist position  $S$  with respect to Exechon's platform point  $P$ ,  $\delta_i^B = (-1, 1), i \in \{1, 2\}$  is chosen. The univocal parameters with the working modes are shown in Fig. (4a), Fig. (4c) and presented in Eq. (1), (2), (3), (4) and Eq. (5).

$$c_\alpha = \left( -\delta_1^B S_x \sqrt{t_0^2 - h_x^2} + h_x S_z \right) / t_0^2 \quad (1)$$

$$s_\alpha = \left( \delta_1^B S_z \sqrt{t_0^2 - h_x^2} + h_x S_z \right) / t_0^2 \quad (2)$$

$$c_\beta = \delta_2^B t_6 / \sqrt{t_6^2 + S_y^2} \quad (3)$$

$$s_\beta = -\delta_2^B S_y / \sqrt{t_6^2 + S_y^2} \quad (4)$$

$$h = \left( \delta_2^B \left( S_y^2 + \delta_1^B t_6 \sqrt{t_0^2 - h_x^2} \right) / \sqrt{t_6^2 + S_y^2} \right) - h_z \quad (5)$$

where  $t_6 = \left( \delta_1^B (t_0^2 - d^B S_x) \sqrt{(t_0^2 - h_x^2)} + d^B h_x S_z \right) / t_0^2$ ,  $t_0^2 = \sqrt{S_x^2 + S_z^2}$ . The above equations are rearranged in a matrix form to represent the transformation from base frame  $O\mathbf{ib}\mathbf{jb}\mathbf{kb}$  to the

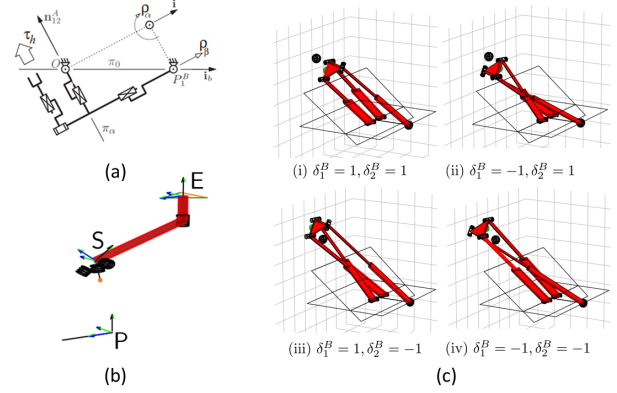


**FIGURE 4:** (a) Equivalent Mechanism with a quasi-serial linkage. Twist around  $\ell(\rho_\alpha) = \mathbf{j}_b, \ell(\rho_\beta) = \mathbf{k}_2^A, \ell(\tau_h) = \mathbf{n}_{12}^A = \mathbf{e}_h$  [16], (b) Serial linkage, (c) Working modes of Exechon PKM

platform  $\mathbf{Pijk}$ , which would aid in computing the IK of the serial chain. The transformation matrix is represented as follows

$${}^P H_O = \begin{bmatrix} s_\alpha & 0 & c_\alpha & 0 \\ -s_\beta c_\alpha & c_\beta & s_\beta s_\alpha & c_\alpha d^B s_\beta \\ -c_\beta c_\alpha & -s_\beta & c_\beta s_\alpha & -h \\ 0 & 0 & 0 & 1 \end{bmatrix} \quad (6)$$

The prismatic actuator joint lengths are computed using Eq. (7) and Eq. (8). Thereby, we derive the actuator stroke necessary to achieve the desired platform pose.

$$q^B = \sqrt{t_1^2 + t_2^2} \quad (7)$$

$$q^L = \sqrt{(t_3 - p^L s_\beta - h^L c_\beta)^2 + (t_2 s_\beta - p^L c_\beta + h^L s_\beta + d^L)^2} \quad (8)$$

where  $L = (A, C)$ ,  $t_1 = d^B s_\alpha - p^B$ ,  $t_2 = d^B c_\alpha + h$ ,  $t_3 = d^B c_\alpha - t_2 c_\beta$ .

There are four working modes as described in [14] for Exechon architecture. From the working prototype Fig. (1) and Fig. (4c), it is evident that we can assume  $\delta_1^B, \delta_2^B = 1$  to represent the prototype architecture. The parameters of the parallel robot geometry are provided in Table. (1).

## 2.2 Reachable Workspace Boundary: Exechon

Parallel manipulators have limited workspace usually constrained by the mechanical limits of the passive joints in each limb, limited actuation range, and singularities that exist due to their kinematic structure. In addition, for a hybrid manipulator

**TABLE 1:** Geometric parameter table for the parallel module

$d^A$	$d^B$	$d^C$	$h_x$
-0.05 m	0.18 m	0.05 m	0 m
$h_z$	$p^A$	$p^B$	$p^C$
0.09 m	-0.05 m	0.086 m	0.05 m

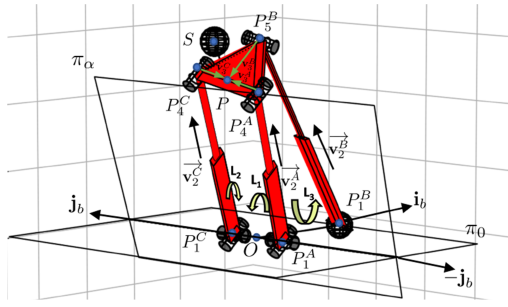


**FIGURE 5:** Loop closures for the Exechon Tripod. Loop 1 ( $L_1$ ):  $OP_1^A + \mathbf{v}_2^A + \mathbf{v}_3^A + PO = 0$ , Loop 2 ( $L_2$ ):  $OP_1^C + \mathbf{v}_2^C + \mathbf{v}_3^C + PO = 0$ , Loop 3 ( $L_3$ ):  $OP_1^B + \mathbf{v}_2^B + \mathbf{v}_3^B + PO = 0$ .

which relies on the parallel linkage for the positioning system, it is essential to characterize the reachable workspace of the PKM. The reachable workspace of the PKM will define the operating workspace of the complete hybrid manipulator. Researchers have presented the workspace of Exechon architecture [17] and its variant using sliced partition algorithms [18]. In [19], workspace of the ideal Exechon robot is used to analyze the effects due to offsets between the axes of joints that connect the limbs of the Exechon manipulator to the fixed frame.

The reachable workspace of the robot,  $W \subset \mathbb{R}^3$ , is a subspace that can be reached by the reference point with at least one orientation of the end-effector [20]. In this paper, the reachable workspace boundary is computed using a state-of-the-art numeric solver *CuikSuite* [21] [22] based on branch and prune technique. The solver utilizes multi-core implementation to obtain the whole real solution set of the boundary points. The current formulation to obtain the boundary set, takes into account both the active and passive joint limit constraints. It is necessary to formulate a system of quadratic equations that characterize the solution set of the boundary. We exploit the univocal parameters  $\alpha$  and  $\beta$  to define the system of quadratic equations. Loop closure equations are formulated to compute the platform pose based on these joint angles. With reference to Fig. (5), loop closure constraints are obtained for each leg ( $L=A, B, C$ ) and the

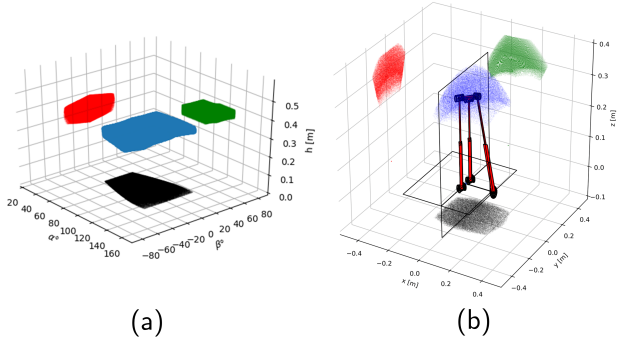


**FIGURE 6:** a) Univocal pose representation for any configuration of the parallel manipulator b) Reachable workspace for the geometrical constraints with IK:  $q^A, q^B, q^C \in [0.240, 0.390]$  m,  $\alpha \in [1.0472, 2.0944]$  rad,  $\beta \in [-0.523599, 0.523599]$  rad

platform point  $P$  respectively. It is of the form:

$$P_{1,i}^L + v_{2,i}^L + v_{3,i}^L - OP_i = 0, \quad i \in \{x, y, z\} \quad (9)$$

The length of the vectors  $v_2^A, v_2^B, v_2^C$  as shown in Fig. (5) are bounded by  $q^A, q^B, q^C$  and lengths of vector  $v_3^A, v_3^B$ , and  $v_3^C$  are based on the geometry of the platform  $p^A, p^B, p^C$ , specified in Table (1) respectively. Hence, the constraint equations are formulated in Eqn. (10-15). The actuator joint lengths are directly bounded by their maximal and minimal values, based on the hardware prototype. We define the bounds as follows:

$$(v_{2,x}^i)^2 + (v_{2,y}^i)^2 + (v_{2,z}^i)^2 - (q^i)^2 = 0 \quad (10)$$

$$(v_{3,x}^i)^2 + (v_{3,y}^i)^2 + (v_{3,z}^i)^2 - (p^i)^2 = 0 \quad (11)$$

$$i \in (A, B, C), (q^A, q^B, q^C) \in [0.240, 0.390]$$

$$v_{3,x}^A + (p^A)(c_\alpha)(s_\beta) = 0 \quad (12)$$

$$v_{3,y}^A - (p^A)(c_\beta) = 0 \quad (13)$$

$$v_{3,z}^A - (p^A)(s_\alpha)(s_\beta) = 0 \quad (14)$$

$$v_3^A = -v_3^C \quad (15)$$

Vector  $\mathbf{v}_3^B$  is normal to the plane  $\pi_\alpha$  and is formulated as

$$\begin{aligned} v_{3,x}^B + (p^B)(s_\alpha) &= 0 \\ v_{3,z}^B + (p^B)(c_\alpha) &= 0 \end{aligned} \quad (16)$$

The angles  $\alpha$  and  $\beta$  are constrained to a unit circle as follows

$$\begin{aligned} c_\alpha^2 + s_\alpha^2 - 1 &= 0 \\ c_\beta^2 + s_\beta^2 - 1 &= 0 \end{aligned} \quad (17)$$

To obtain the workspace boundary, there are three main mechanical constraints that limit the workspace: (i) actuator's stroke (ii) range of the passive joints, and (iii) link interference [23].

### 2.2.1 Range of actuator stroke and passive joints

The parallel manipulator has an actuator stroke of 150 mm. The actuator joints  $q^A$ ,  $q^B$  and  $q^C$  are bounded to be within the range of [0.240,0.390] m based on the manipulator design. The passive joints have a limited range, hence restricting the corresponding manipulator motion. The rotation of platform around the legs A and C around  $\xi_2^A$  and  $\xi_2^C$  attached to the platform is limited to  $\pm 30^\circ$  and leg B is limited to  $\pm 50^\circ$  respectively. Similarly, the legs A and C attached to the upper platform has rotations in the range of  $[-30^\circ, 40^\circ]$ , while leg B mounted on a spherical joint can achieve rotations of  $[-50^\circ, 50^\circ]$ . The boundary conditions for accurate workspace determination is derived in this section. Mechanical limits on the joints can be easily modeled as equality constraints. The distance and angular constraints are added for prismatic and revolute joints. The mechanical joint limits for the parallel manipulator are modelled as shown in Eqn. (18).

$$\prod_{i=1}^3 f_i t_i g_i = 0 \quad (18)$$

$$f_i \in [-w_i, w_i]$$

$$t_i \in [-\sqrt{q_{max}^i - q_{max}^i \cos(\max(\gamma_i^x))}, \sqrt{q_{max}^i - q_{max}^i \cos(\max(\gamma_i^x))}]$$

$$g_i \in [-\sqrt{q_{max}^i - q_{max}^i \cos(\max(\gamma_i^y))}, \sqrt{q_{max}^i - q_{max}^i \cos(\max(\gamma_i^y))}]$$

For a joint distance  $q_i$  that satisfies the lower and upper bound, the constraints are as in Eqn. (19-21). The values  $m_i$  and  $h_i$  are called the mid-point and half-range of the interval and the first equation (Eq. 19) simply constrains the pairs  $(q_i, f_i)$  to take values on a circle of radius  $h_i$  centered at  $(m_i, 0)$  in the  $(q_i, f_i)$  plane. Additional constraints are included for the workspace determination using the working mode parameters.

$$(q^i - m_i)^2 + f_i^2 - w_i^2 = 0 \quad (19)$$

$$m_i = (q_{max}^i + q_{min}^i)/2 \quad (20)$$

$$w_i = (q_{max}^i - q_{min}^i)/2 \quad (21)$$

The values of constraint parameters used in the boundary determination are given as  $m_i = 0.315$  m,  $h_i = 0.075$  m,  $f_i \in [-0.075, 0.075]$  and  $(v_{j,x}^i, v_{j,y}^i, v_{j,z}^i \in [-1, 1])$ . Passive joint constraints are modelled as

$$c_{\gamma_i^x}(\sqrt{(v_{2,x}^i)^2 + (v_{2,z}^i)^2}) - v_{2,z}^i = 0 \quad (22)$$

$$c_{\gamma_i^x}(\sqrt{(v_{2,y}^i)^2 + (v_{2,z}^i)^2}) - v_{2,z}^i = 0 \quad (23)$$

$$c_{\gamma_i^x} = g_i^2 + \cos(\max(\gamma_i^x)) \quad (24)$$

$$c_{\gamma_i^y} = h_i^2 + \cos(\max(\gamma_i^y)) \quad (25)$$

$$c_{\gamma_i^y}^2 + s_{\gamma_i^y}^2 - 1 = 0 \quad (26)$$

$$c_{\gamma_i^y}^2 + s_{\gamma_i^y}^2 - 1 = 0 \quad (27)$$

To choose the actual working mode parameter ( $r_1 \in$

$[0, p^A]$ ,  $r_2 \in [0, p^C]$ ,  $r_3 \in [0, p^B]$ ) to represent the prototype, a system of equation are defined as follows

$$v_{2,y}^C + P_{1,y}^C - y - r_1 = 0 \quad (28)$$

$$y - v_{2,y}^A - P_{1,y}^A - r_2 = 0 \quad (29)$$

$$v_{2,x}^B + P_{1,x}^B - x - r_3 = 0 \quad (30)$$

Fig. (8) shows the reachable workspace of the parallel chain with geometric constraints that was validated using *CukSuite*. The results obtained were similar to the sliced partition approach to determine the complete workspace using dense discretization and IK computation as shown in Fig. (6). Fig. (6a) also shows the subsequent range of the univocal parameters within the reachable workspace, which can aid in numerical optimization for forward kinematics. A mathematical mock-up of the hybrid architecture has been created using Python 3.8 to automatically generate the parametric figures.

### 2.3 Position Kinematics of Serial Chain: Forward and Inverse Problem

The forward kinematic problem of the 4-DOF spherical revolute (SR) chain as shown in Fig. (4b), is to find the position and orientation of the reference frame attached to the end-effector  $E$  given the joint position set. The spherical wrist consists of three intersecting revolute joints, which are orthogonal to each other.

**TABLE 2:** Geometric parameter table for Serial Arm

$e_x^S$ (m)	$e_z^S$ (m)	$e_z^D$ (m)	
0.3253	-0.2645	-0.1173	
$\Theta$	$\theta_1$ (rad)	$\theta_2$ (rad)	$\theta_3$ (rad)
$-45^\circ$	[-2.40, 2.90]	[0.10, -1.00]	[-2.0, 2.0]

The IK problem of the entire 3+4 hybrid robot is to find three prismatic joint lengths of the platform and four revolute joint values of the top serial-chain arm such that the end-effector frame  $E$  of the entire robot can meet a desired pose. The problem is decomposed into two parts (a) solving the IK of the parallel manipulator first and obtaining the platform pose  $P$ , (b) Secondly, with the assumption that the current wrist point  $S$  is known based on the geometry, we derive the input angles for the spherical revolute wrist linkage and PKM actuator stroke to obtain the desired end-effector pose  $E$ , thereby solving the whole kinematic chain. The end-effector is represented using ZYZ euler angle convention  ${}^0H_E$ . The position  $P_4^D$  of the fourth revolute joint axis is first determined, where  $P_4^D$  is  $[0, 0, e_z^D]$  in end effector frame  $Ei_e j_e k_e$ . Revolute joint  $\ell(\xi_4^D)$  is at an angle  $\Theta$  along  $k_2^S$  and offset by

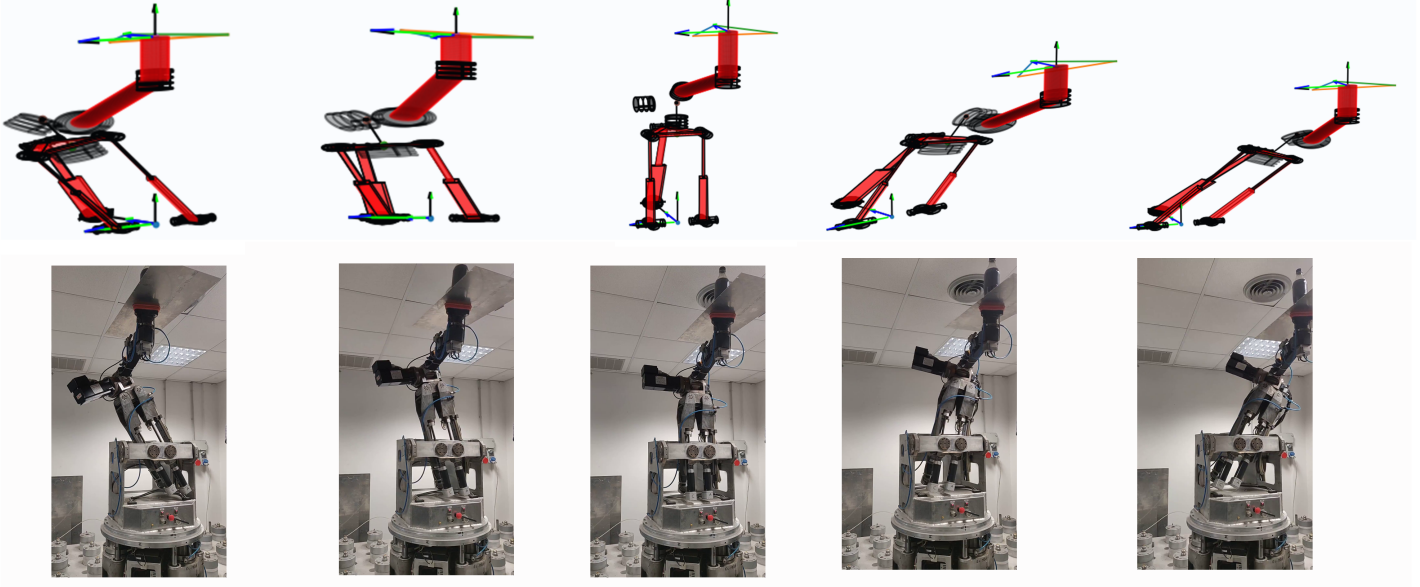


**FIGURE 7:** Simulation (above) and prototype snapshots (below) of straight line motion generation experiments of the hybrid robot, captured at every 10s

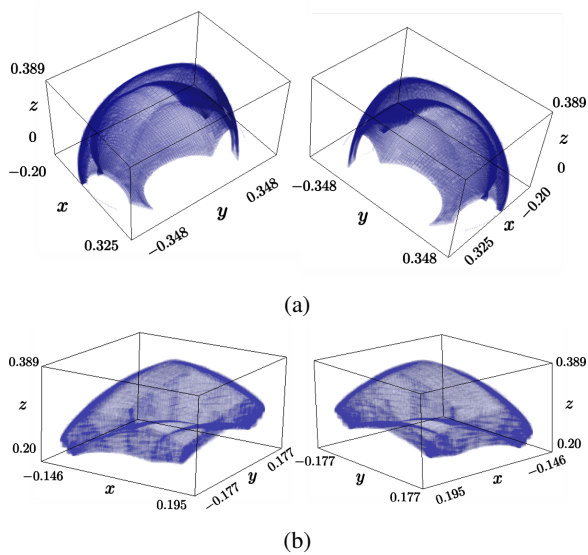


**FIGURE 8:** Reachable workspace boundary, (a) With active joint limits and with working mode parameter,  $q^A, q^B, q^C \in [0.240, 0.390]\text{m}$ ,  $OP_z \geq 0$ ,  $\delta_1^B \delta_1^B = 1$ , (b) With active and passive joint limits  $q^A, q^B, q^C \in [0.240, 0.390]\text{m}$ ;  $OP_z \geq 0$ ,  $\delta_1^B \delta_2^B = 1$ ;  $\gamma_i^x, \gamma_i^y \in [\pm 30^\circ, \pm 50^\circ, \pm 30^\circ]$ ,  $i \in \{A, B, C\}$

$[e_x^S, 0, e_z^S]$  from the center of the spherical wrist by construction, which helps to obtain  ${}^E H_S$ . Since the current spherical wrist position is a known-priori, based on  $P_4^D$  and current position of  $S$ , we can derive the desired wrist intersection position. Hence the desired wrist center can be computed trivially by concatenation of individual transformation matrices. After obtaining the desired spherical wrist position by computing the IK for the Exechon PKM using Eq. (1-5) and checking the feasibility of the joint limits, we continue to obtain the actuator angles for the spherical wrist using Algorithm I. The geometric parameters of the serial module are shown in Table (2). The methodology in Algorithm I can be adapted with minimal reformulation to compute inverse kinematics for a parallel-serial architecture, given that the current pose of the parallel manipulator is known and the serial manipulator is an orthogonal spherical wrist.

### 3 Trajectory Planning of hybrid parallel-serial robot

The scheme of trajectory generation is to compute for the control system, the desired reference joint or end-effector variables as functions of time such that hybrid robot tracks the desired path. The task space approach to trajectory generation is illustrated in the Fig. (9). The superscripts i and f designate the initial and final values respectively. The hybrid robot controller

---

**Algorithm 1** Serial chain IK Solver

---

**Require:** Pose of end-effector  $E^0H_E$  in Base Frame  $(E_x, E_y, E_z, \phi, \theta, \psi)$ , Current serial joint states  $(\theta_1^c, \theta_2^c, \theta_3^c)$

**Ensure:** Joint configurations  $(\theta_1, \theta_2, \theta_3)$

**function** Serial\_IK\_Serial\_Solver( ${}^0H_E, E$ )

```

 ${}^0H_S = ({}^0H_E)({}^E H_S)$            ▷  $4 \times 4$  Homogeneous matrix
 ${}^P H_S = ({}^P H_O)({}^0 H_S)$          ▷  $4 \times 4$  Homogeneous matrix
if  $t == 0$  then                      ▷ At time  $t = 0$  or first iteration
     $\theta_1^c, \theta_2^c, \theta_3^c = [0, 0, 0]$ 
end if
if  ${}^P H_S(3,3) == 1$  then
     $\theta_1 = \theta_1^c$                    ▷ Multiple solutions: Only  $\theta_1 + \theta_3$  computed
     $\theta_2 = 0$ 
     $\theta_3 = \text{atan2}\left({}^P H_S(2,1), {}^P H_S(1,1)\right) - \theta_1$ 
else if  ${}^P H_S(3,3) == -1$  then
     $\theta_1 = \theta_1^c$                    ▷ Multiple solutions: Only  $\theta_1 - \theta_3$  computed
     $\theta_2 = \pi$ 
     $\theta_3 = \text{atan2}\left(-{}^P H_S(1,2), -{}^P H_S(1,1)\right) + \theta_1$ 
else                                     ▷ Two possible solutions
     ${}^1\theta_1 = \text{atan2}\left({}^P H_S(2,3), {}^P H_S(1,3)\right)$ 
     ${}^1\theta_2 = \text{atan2}\left(\sqrt{1 - ({}^P H_S(3,3))^2}, {}^P H_S(3,3)\right)$ 
     ${}^1\theta_3 = \text{atan2}\left({}^P H_S(3,2), -{}^P H_S(3,1)\right)$ 
     $d_{\max}^1 = \max\left(\left|{}^1\theta_1 - \theta_1^c\right|, \left|{}^1\theta_2 - \theta_2^c\right|, \left|{}^1\theta_3 - \theta_3^c\right|\right)$ 
     ${}^2\theta_1 = \text{atan2}\left(-{}^P H_S(2,3), -{}^P H_S(1,3)\right)$ 
     ${}^2\theta_2 = \text{atan2}\left(-\sqrt{1 - ({}^P H_S(3,3))^2}, {}^P H_S(3,3)\right)$ 
     ${}^2\theta_3 = \text{atan2}\left(-{}^P H_S(3,2), {}^P H_S(3,1)\right)$ 
     $d_{\max}^2 = \max\left(\left|{}^2\theta_1 - \theta_1^c\right|, \left|{}^2\theta_2 - \theta_2^c\right|, \left|{}^2\theta_3 - \theta_3^c\right|\right)$ 
if  $d_{\max}^1 < d_{\max}^2$  then
     $\theta_1 = {}^1\theta_1, \theta_2 = {}^1\theta_2, \theta_3 = {}^1\theta_3$ 
     $\theta_1^c = {}^1\theta_1, \theta_2^c = {}^1\theta_2, \theta_3^c = {}^1\theta_3$ 
else
     $\theta_1 = {}^2\theta_1, \theta_2 = {}^2\theta_2, \theta_3 = {}^2\theta_3$ 
     $\theta_1^c = {}^2\theta_1, \theta_2^c = {}^2\theta_2, \theta_3^c = {}^2\theta_3$ 
end if
end if
return  $\theta_1, \theta_2, \theta_3$ 

```

---

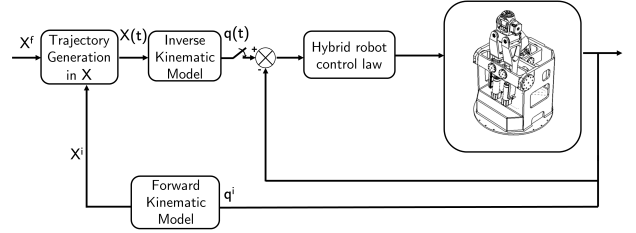


**FIGURE 9:** Trajectory generation in the Cartesian space for the hybrid robot

executes a time-synchronized motion path, which is a third order interpolation between the actual and the next reference point, after receiving a set of interpolation points from the higher-level trajectory planner represented by PVT points, each of which contains information on the position, velocity, and time of a trajectory segment end point. The trajectory that was realized by the hybrid robot is a linear interpolation between two postures defined by two angles and by three Cartesian coordinates  $x, y, z$  for which the velocity is specified as a ratio of maximum velocity. A third degree polynomial is used to define the position, velocity and acceleration along a linear interpolation as given by Eqn. (31). A parabolic velocity profile is obtained using a cubic polynomial that ensures continuity of velocity but not of acceleration. This discontinuity is filtered by the mechanical structure due to a sufficiently rigid robot design.

$$\begin{aligned} r(t) &= 3\left(\frac{t}{t_f}\right)^2 - 2\left(\frac{t}{t_f}\right)^3 \\ \dot{r}(t) &= 6\left(\frac{t}{t_f^2}\right) - 6\left(\frac{t^2}{t_f^3}\right) \\ \ddot{r}(t) &= 6\left(\frac{1}{t_f^2}\right)^2 - 12\left(\frac{t}{t_f^3}\right) \end{aligned} \quad (31)$$

For a linear trajectory, the minimum travelling time  $t_f$  is defined as in [24]. Let  $\mathbf{P}_1$  and  $\mathbf{P}_2$  represent the vectors defining the first and second pose of the hybrid robot's end-effector, respectively. Any intermediate pose  $\mathbf{P}$ , velocity vector  $\mathbf{V}(t)$  and the acceleration vector  $\mathbf{A}(t)$  is denoted as:

$$\mathbf{P}(t) = \mathbf{P}_1 + (\mathbf{P}_2 - \mathbf{P}_1)\mathbf{r}(t) \quad (32)$$

$$\mathbf{V}(t) = \dot{\mathbf{r}}(t)(\mathbf{P}_2 - \mathbf{P}_1) \quad (33)$$

$$\mathbf{A}(t) = \ddot{\mathbf{r}}(t)(\mathbf{P}_2 - \mathbf{P}_1) \quad (34)$$

The corresponding joint coordinate vector is obtained by:

$$\mathbf{q}(t) = \mathbf{f}(\mathbf{P}(t)) \quad (35)$$

where  $\mathbf{f}$  denotes the inverse geometric model of the hybrid parallel robot. The joint velocities and joint acceleration are determined using the inverse kinematic Jacobian matrix and its derivative respectively.

Fig. (7) and (10) shows the simulation and experimental

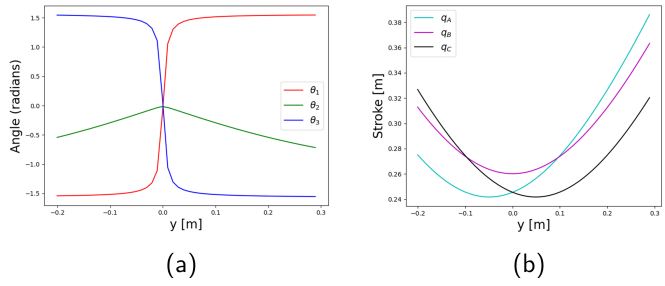


**FIGURE 10:** Results of trajectory generation performance evaluation (a) Joint positions of serial chain (b) Joint positions of parallel chain

evaluation of the hybrid robot performing a linear trajectory with its joint values during the complete trajectory. The experiment was carried out by vacuum clamping a sheet metal onto the adaptable tool head and placing a filled bottle on top of the sheet metal, to verify the stability during the motion. The evolution of joint variables of the three joints of the serial spherical chain and the variation of stroke of the prismatic actuators of the parallel chain derived in simulation are shown in Fig. (10a) and Fig. (10b) respectively. The linear trajectory was carried out in XY-plane and we can observe that at  $y = 0\text{m}$ , in Fig. (10), the robot is in a vertical standstill position with minimal stroke from the prismatic actuators of the parallel robot and minimal joint variation in the serial chain as observed in the central image of the top and bottom part of Fig. (7).

#### 4 Conclusion and Future Work

In this paper, we presented the complete parametric model of a novel hybrid parallel-serial architecture with greater kinematic complexity. The parallel manipulator is used as a positioning device and the serial chain consists of a redundant spherical wrist acting as an orientation device. The workspace of the parallel chain and its range of motion were analyzed in detail using branch and prune based numerical solver. The system of equations for the numerical solver were derived using the univocal parametric representation and loop-closure equations. The complete workspace boundary was presented for the generic Exechon architecture and also by taking into account, the complete set of mechanical constraints. Trajectory generation and curve tracing using the kinematic formulation were tested and successfully implemented on the hybrid manipulator prototype. Future work will explore kinematic control techniques for task-based planning, such as fixturing, where the redundancy in the hybrid architecture will aid to achieve feasible solutions in tightly constrained environments.

#### ACKNOWLEDGMENT

The first author has received funding from the European Union’s Horizon 2020 research and innovation programme under the Marie Skłodowska Curie grant agreement No. 847402.

#### REFERENCES

- [1] Kumar, R., Kumar, S., Müller, A., and Kirchner, F., 2022. “Modular and hybrid numerical-analytical approach-a case study on improving computational efficiency for series-parallel hybrid robots”. In 2022 IEEE/RSJ International Conference on Intelligent Robots and Systems (IROS), IEEE, pp. 3476–3483.
- [2] Kumar, S., Wörle, H., de Gea Fernández, J., Müller, A., and Kirchner, F., 2020. “A survey on modularity and distributivity in series-parallel hybrid robots”. *Mechatronics*, **68**, p. 102367.
- [3] Zhou, B., and Xu, Y., 2007. “Robust control of a 3-dof hybrid robot manipulator”. *The International Journal of Advanced Manufacturing Technology*, **33**(5-6), pp. 604–613.
- [4] Merlet, J.-P., 2006. *Parallel robots*, Vol. 128. Springer Science & Business Media.
- [5] Kong, X., and Gosselin, C., 2007. *Virtual-Chain Approach for the Type Synthesis of Parallel Mechanisms*. Springer.
- [6] Romdhane, L., 1999. “Design and analysis of a hybrid serial-parallel manipulator”. *Mechanism and Machine Theory*, **34**(7), pp. 1037–1055.
- [7] Tanev, T. K., 2000. “Kinematics of a hybrid (parallel-serial) robot manipulator”. *Mechanism and Machine Theory*, **35**(9), pp. 1183–1196.
- [8] Lee, M. K., Park, K. W., and Choi, B. O., 1999. “Kinematic and dynamic models of hybrid robot manipulator for propeller grinding”. *Journal of Robotic Systems*, **16**(3), pp. 137–150.
- [9] Huang, M. Z., Ling, S.-H., and Sheng, Y., 1993. “A study of velocity kinematics for hybrid manipulators with parallel-series configurations”. In Robotics and Automation, 1993. Proceedings., 1993 IEEE International Conference on, IEEE, pp. 456–461.
- [10] Campos, A., Budde, C., and Hesselbach, J., 2008. “A type synthesis method for hybrid robot structures”. *Mechanism and Machine Theory*, **43**(8), pp. 984–995.
- [11] Bi, Z. M., and Jin, Y., 2011. “Kinematic modeling of exechon parallel kinematic machine”. *Robotics and Computer-Integrated Manufacturing*, **27**(1), pp. 186–193.
- [12] Trinh, C., Zlatanov, D., and Zoppi, M., 2016. “Direct kinematics of the exechon tripod”. In ASME 2016 International Design Engineering Technical Conferences and Computers and Information in Engineering Conference, American Society of Mechanical Engineers, pp. V05BT07A092–V05BT07A092.

- [13] Cuong, T. D., 2018. “Geometric perspective on kinematics and singularities of spatial mechanisms”.
- [14] Zoppi, M., Zlatanov, D., and Molfino, R., 2010. “Kinematics analysis of the exechon tripod”. In ASME 2010 international design engineering technical conferences and computers and information in engineering conference, American Society of Mechanical Engineers, pp. 1381–1388.
- [15] Exechon homepage. <http://www.exechon.com>. Accessed: 2018-12-16.
- [16] Zlatanov, D., Zoppi, M., and Molfino, R., 2012. “Constraint and singularity analysis of the exechon tripod”. In ASME 2012 international design engineering technical conferences and computers and information in engineering conference, American Society of Mechanical Engineers, pp. 679–688.
- [17] Jin, Y., Bi, Z. M., Liu, H., Higgins, C., Price, M., Chen, W., and Huang, T., 2015. “Kinematic analysis and dimensional synthesis of exechon parallel kinematic machine for large volume machining”. *Journal of Mechanisms and Robotics*, 7(4), p. 041004.
- [18] Tengfei, T., Yanqin, Z., Jun, Z., and Yan, J., 2016. “Conceptual design and workspace analysis of an exechon-inspired parallel kinematic machine”. In *Advances in Reconfigurable Mechanisms and Robots II*. Springer, pp. 445–453.
- [19] López-Custodio, P., Dai, J., Fu, R., and Jin, Y., 2020. “Kinematics and constraints of the exechon robot accounting offsets due to errors in the base joint axes”. *Journal of Mechanisms and Robotics*, 12(2).
- [20] Kumar, A., and Waldron, K., 1981. “The workspaces of a mechanical manipulator”. *Journal of Mechanical Design*, 103(3), pp. 665–672.
- [21] Porta, J. M., Ros, L., Bohigas, O., Manubens, M., Rosales, C., and Jaillet, L., 2014. “The cuik suite: Analyzing the motion closed-chain multibody systems”. *IEEE Robotics & Automation Magazine*, 21(3), pp. 105–114.
- [22] Müller, A., and Zlatanov, D., 2019. *Singular Configurations of Mechanisms and Manipulators*. Springer.
- [23] Bonev, I. A., and Ryu, J., 2001. “A new approach to orientation workspace analysis of 6-dof parallel manipulators”. *Mechanism and machine theory*, 36(1), pp. 15–28.
- [24] Khalil, W., and Dombre, E., 2002. *Modeling identification and control of robots*. CRC Press.

$\mathbf{n}_{12}^L$	unit vector with direction $\mathbf{k}_1^L \times \mathbf{k}_2^L, L = A, C$
$\pi_\alpha$	plane through $\ell(\xi_1^A)$ and normal to $\mathbf{k}_4^A$
$\pi_h$	plane containing $\ell(\xi_5^B)$ and parallel to $\ell(\xi_4^A), \ell(\xi_4^C)$
$e_h$	unit vector orthogonal to $\pi_h$ with the direction of $\mathbf{k}_2^A \times \mathbf{k}_5^B$
$P_1^L$	point on $\ell(\xi_1^L)$ and its common normal with $\ell(\xi_2^L), L = A, C$
$P_2^L$	projection of $P_1^L$ on $\ell(\xi_2^L), L = A, C$
$P_4^L$	projection of $P_2^L$ on $\ell(\xi_4^L), L = A, C$
$P_1^B$	center of the S joint
$P_5^B$	projection of $P_1^B$ on $\ell(\xi_5^B)$
$P$	projection of $P_5^B$ on $\pi_\alpha$
$P_4^D$	point on $\ell(\xi_4^D)$
$O$	projection of $P_1^B$ on $\ell(\xi_1^A)$
$\pi_e^B$	plane through $P_1^B$ orthogonal to $\mathbf{k}_5^B$
$S$	point on $\pi_e^B$
$\pi_0$	plane of $\ell(\xi_1^A)$ and $P_1^B$ ; if $P_1^B \in \ell(\xi_1^A)$ any plane of the pencil
$\alpha$	angle between $\pi_\alpha$ and $\pi_0$ positive about $\mathbf{j}_b$
$\beta$	angle between $\mathbf{k}_5^B$ and $\mathbf{k}_1^A$ positive about $\mathbf{k}_2^A$
$h$	distance of $O$ from $\pi_h$ with sign according to $e_h$
$O\mathbf{i}_b\mathbf{j}_b\mathbf{k}_b$	reference frame at $O$ with $\mathbf{i}_b \perp \mathbf{k}_1^A, \mathbf{j}_b = \mathbf{k}_1^A, \mathbf{k}_b \perp \pi_0$
$P\mathbf{i}\mathbf{j}\mathbf{k}$	reference frame at $P$ with $\mathbf{i} = \mathbf{k}_2^A, \mathbf{j} = \mathbf{k}_5^B, \mathbf{k} = e_h$
$E\mathbf{i}_e\mathbf{j}_e\mathbf{k}_e$	reference frame on the end-effector $E$
$S\mathbf{i}_s\mathbf{j}_s\mathbf{k}_s$	reference frame at spherical joint $S$
$\phi, \theta, \psi$	Precession, nutation, and spin angle in <b>xyz</b> euler convention, representing the body orientation of the end effector $E$ reference frame in $O$
$\Theta$	Orientation of frame $S$ with reference to frame $E$
$v_2^L$	vector between points, $P_2^L$ and $P_4^L, L = A, C$
$v_2^B$	vector between points, $P_1^B$ and $P_5^B, L = A, C$
$v_3^L$	vector between points, $P_4^L$ and $P, L = A, C$
$v_3^B$	vector between points, $P_5^B$ and $P, L = A, C$
$h^L$	distance from $\ell(\xi_4^L)$ to $\pi_h, L = A, C$ , sign according to $e_h$
$l_{12}^L$	distance between $\ell(\xi_1^L)$ and $\ell(\xi_2^L), L = A, C$
$\delta_1^B, \delta_2^B$	working mode parameters when the end-effector pose is assigned by $S (= \pm 1), \delta^L \pm 1$ , for leg $L = A, C$
$h_x, h_z$	respectively: $\mathbf{i}$ and $\mathbf{k}$ coordinates of $S$ in $P\mathbf{i}\mathbf{j}\mathbf{k}$
$d^A, d^B, d^C$	respectively: $\mathbf{j}_b$ coordinate of $P_1^A$ , $\mathbf{i}_b$ coordinate of $P_1^B$ , $\mathbf{j}_b$ coordinate of $P_1^C$ , in $O\mathbf{i}_b\mathbf{j}_b\mathbf{k}_b$
$p^A, p^B, p^C$	respectively: $\mathbf{j}$ coordinate of $P_4^A$ , $\mathbf{i}$ coordinate of $P_5^B$ , $\mathbf{j}$ coordinate of $P_4^C$ , in $P\mathbf{i}\mathbf{j}\mathbf{k}$
$e_x^S, e_y^S, e_z^S$	respectively: $\mathbf{i}_e$ coordinate of $S$ , $\mathbf{k}_e$ coordinate of $S$ , $\mathbf{k}_e$ coordinate of $P_4^D$ in $E\mathbf{i}_e\mathbf{j}_e\mathbf{k}_e$
$P_{n,x}^L, P_{n,y}^L, P_{n,z}^L$	respectively: $\mathbf{i}, \mathbf{j}, \mathbf{k}$ component of vector $\overrightarrow{OP_n^L}$ in $O\mathbf{i}_b\mathbf{j}_b\mathbf{k}_b$ , where $n = (1, 2, 3), L = (A, B, C)$
$OP_x^L, OP_y^L, OP_z^L$	respectively: $\mathbf{i}, \mathbf{j}, \mathbf{k}$ component of vector $\overrightarrow{OP}$ in $O\mathbf{i}_b\mathbf{j}_b\mathbf{k}_b$ , where $L = (A, B, C)$
$v_{n,x}^L, v_{n,y}^L, v_{n,z}^L$	respectively: $\mathbf{i}, \mathbf{j}, \mathbf{k}$ component of vector $\overrightarrow{v_n^L}$ in $O\mathbf{i}_b\mathbf{j}_b\mathbf{k}_b$ , where $n = (2, 3), L = (A, B, C)$

## NOMENCLATURE

- $s_\gamma, c_\gamma$   $\sin\gamma, \cos\gamma$
- $A, C$  labels of the RRPR legs
- $B$  labels of the SPR leg
- $L$  generic leg,  $L = A, B, C, D$
- $\xi_i^L$  normalized unit twist of the  $i$ -th joint of the leg  $L$
- $\ell(\xi)$  axis of a finite-pitch twist
- $\mathbf{k}_i^L$  unit vector parallel to  $\ell(\xi_i^L), L = A, C, D$